# Mechanism of Aldehyde Oxidation Catalyzed by Horse Liver Alcohol Dehydrogenase†

Leif P. Olson, Jia Luo, Örn Almarsson, and Thomas C. Bruice*

*Department of Chemistry, University of California at Santa Barbara, Santa Barbara, California 93106*

*Received August 24, 1995; Revised Manuscript Received May 3, 1996*⊗

ABSTRACT: The mechanism of oxidation of benzaldehyde to benzoic acid catalyzed by horse liver alcohol dehydrogenase (HLADH) has been investigated using the HLADH structure at 2.1 Å resolution with $NAD^+$ and pentafluorobenzyl alcohol in the active site [Ramaswamy et al. (1994) *Biochemistry 33*, 5230−5237]. Constructs for molecular dynamics (MD) investigations with HLADH were obtained by a best-fit superimposition of benzaldehyde or its hydrate on the pentafluorobenzyl alcohol bound to the active site Zn(II) ion. Equilibrium bond lengths, angles, and dihedral parameters for Zn(II) bonding residues His67, Cys46, and Cys174 were obtained from small-molecule X-ray crystal structures and an *ab initio*-derived parameterization of zinc in HLADH [Ryde, U. (1995) *Proteins: Struct., Funct., Genet. 21*, 40−56]. Dynamic simulations in CHARMM were carried out on the following three constructs to 100 ps: (MD1) enzyme with $NAD^+$, benzaldehyde, and zinc-ligated $HO^-$ in the active site; (MD2) enzyme with $NAD^+$ and hydrated benzaldehyde monoanion bound to zinc via the *pro-R* oxygen, with a proton residing on the *pro-S* oxygen; and (MD3) enzyme with $NAD^+$ and hydrated benzaldehyde monoanion bound to zinc via the *pro-S* oxygen, with a proton residing on the *pro-R* oxygen. Analyses were done of 800 sample conformations taken in the last 40 ps of dynamics. Structures from MD1 and MD3 were used to define the initial spatial arrangements of reactive functionalities for semiempirical PM3 calculations. Using PM3, model systems were calculated of ground states and some transition states for aldehyde hydration, hydride transfer, and subsequent proton shuttling. With benzaldehyde and zinc-bound hydroxide ion in the active site, the oxygen of Zn(II)−OH resided at a distance of 2.8−5.5 Å from the aldehyde carbonyl carbon during the dynamics simulation. This may be compared to the PM3 transition state for attack of the Zn(II)−OH oxygen on the benzaldehyde carbonyl carbon, which has an O···C distance of 1.877 Å. HLADH catalysis of the aldehyde hydration would require very little motion aside from that in the ground state. Two simulations of benzaldehyde hydrate ligated to zinc (MD2 and MD3) both showed close approach of the aldehyde hydrate hydrogen to $NAD^+$ C4, varying from 2.3 to 3.3 Å, seemingly favorable for the hydride transfer reaction. The MD2 configuration does not allow proton shuttling. On the other hand, when the *pro-S* oxygen is ligated to zinc (MD3), the proton on the *pro-R* oxygen averages 2.09 Å from the hydroxyl oxygen of Ser48 such that initiation of shuttling of protons via Ser48 to the ribose 2′-hydroxyl oxygen to the 3′-hydroxyl oxygen to His51 nitrogen is sterically favorable. PM3 calculations suggest that this proton shuttle represents a stepwise reaction which occurs subsequent to hydride transfer. The PM3 transition state for hydride transfer based on the MD3 configuration has the transferring hydride 1.476 Å from C4 of $NAD^+$ and 1.433 Å from the aldehyde α-carbon.

Horse liver alcohol dehydrogenase (HLADH,[1] EC 1.1.1.1) is generally associated with the interconversion of alcohols and aldehydes (eq 1; Brändén, et al., 1975). HLADH has also received some attention for its catalysis of aldehyde oxidation (eq 2).

$$\{E/NAD^+/\text{alcohol}\} \rightarrow \{E/NADH/\text{aldehyde}\} \quad (1)$$

$$\{E/NAD^+/\text{aldehyde}\} \rightarrow \{E/NADH/\text{carboxylic acid}\} \quad (2)$$

Each subunit of this dimeric enzyme binds one molecule of NAD(H) and two Zn(II) ions. One zinc is in the active site, while the other is structural. Aldehydes and alcohols ligate to the active site Zn(II).

Two recent reports show that the function of HLADH in aldehyde oxidative metabolism is underappreciated. Henehan and Oppenheimer (1993) studied the reaction of butanal with HLADH by $^1H$ NMR spectroscopy. Lag phases in attainment of equilibria between alcohol and aldehyde in the presence of large amounts of enzyme and/or aldehyde and $NAD^+$ were attributed to the NADH produced by aldehyde oxidation (eq 2) being directly consumed in a reduction of aldehyde (eq 4). Plapp and co-workers obtained rate and equilibrium constants for HLADH catalysis of benzaldehyde oxidation by $NAD^+$ (Shearer et al., 1993). The value of $k_{cat}$ for oxidation of benzaldehyde by HLADH is smaller (0.38

† We express our appreciation to the National Institutes of Health and the Office of Naval Research for support of this study.

* All correspondence regarding the paper should be addressed to Professor Thomas C. Bruice, Department of Chemistry, University of California at Santa Barbara, Santa Barbara, CA 93106. Phone (805) 893-2044. Fax: (805) 893-2229.

⊗ Abstract published in *Advance ACS Abstracts,* July 1, 1996.

[1] Abbreviations: Im, imidazole; HLADH, horse liver alcohol dehydrogenase; MD, molecular dynamics; $NAD^+$, nicotinamide adenine dinucleotide; NADH, 1,4-dihydronicotinamide adenine dinucleotide; Ph, phenyl.

S0006-2960(95)02020-4 CCC: $12.00 

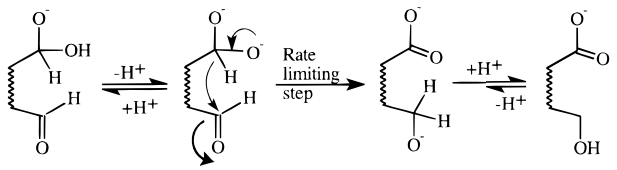


FIGURE 1: Cannizzaro reaction resulting in the oxidation of an aldehyde hydrate to a carboxylic acid. Aldehyde hydration catalyzed by HLADH is an analogous process, with $NAD^+$ serving as the hydride acceptor.

$s^{-1}$, eq 3) than $k_{cat}$ for its reduction (47 $s^{-1}$, eq 4). In aldehyde dismutation (eqs 3 and 4), the binding of benzaldehyde to E/$NAD^+$ ($K_m = 2.5 \times 10^{-3}$ M) is

$$\{E/NAD^+/\text{benzaldehyde}\} \rightarrow \{E/NADH/\text{benzoate}\} \quad (3)$$

$$\{E/NADH/\text{benzaldehyde}\} \rightarrow \{E/NAD^+/\text{benzyl alcohol}\} \quad (4)$$

not as favorable as the binding of benzyl alcohol to E/$NAD^+$ ($K_m = 2.7 \times 10^{-5}$ M).

From a mechanistic standpoint, the reaction of aldehyde with $NAD^+$ is intriguing. Formaldehyde dismutation by HLADH was studied by Abeles and Lee (1960), and the *gem*-diol $H_2C(OH)_2$ was presumed to bind to and react in the enzyme. Formaldehyde exists almost exclusively in the hydrated form in water. Other alcohol dehydrogenases have been shown to possess significant aldehyde oxidation activity, and correlations between reactivity and the propensity of aldehyde substrates to hydrate in aqueous solution have been made in the case of fruit fly alcohol dehydrogenase (Eisses, 1989). Butanal [used in the study of Henehan and Oppenheimer (1993)] and benzaldehyde [used by Shearer et al. (1993)] both exist mainly in the unhydrated keto-form in aqueous solution. An interesting question arises in such cases, as to whether HLADH might catalyze hydrate formation by delivering zinc-bound $HO^-$ to the bound aldehyde substrate (eq 5), in a mechanism with tetracoordinate zinc.

$$RCHO + HO{-}Zn^{2+} \rightarrow RCH(OH)O{-}Zn^{2+} \quad (5)$$

This might occur in addition to complexing zinc directly with the preformed aldehyde hydrate (which exists at some slight equilibrium concentration in water even if hydration is disfavored). The latter possibility might be considered to occur via formation of a pentacoordinate Zn(II) species (associative mechanism) or a tricoordinate Zn(II) species with loss of zinc-bound water.

If HLADH catalyzes the critical first step of hydrate formation, this would constitute an interesting parallel of its aldehyde dehydrogenase activity with that of "true" aldehyde dehydrogenases. Some aldehyde dehydrogenases have been shown to have a cysteine residue which is necessary for catalysis (Fárres et al., 1995). It is believed that this conserved cysteine in aldehyde dehydrogenases attacks the aldehyde group to form a covalently linked enzyme/substrate thiohemiacetal intermediate, from which a hydride is delivered to $NAD^+$ or $NADP^+$ (Hempel et al., 1993; Wang & Weiner, 1995; Fárres et al., 1995). It is conceivable that nucleophilic attack by cysteine in aldehyde dehydrogenases might be mirrored by zinc-bound hydroxide ion in HLADH.

Intramolecular Cannizzaro reactions of aldehyde hydrates lacking enolizable hydrogens (Figure 1) provide an analogy to the enzymatic reaction insofar that the rate of hydride transfer from aldehyde hydrate to the hydride acceptor is enhanced relative to the intermolecular variant (Bowden, 1990). The aldehyde oxidation reaction of HLADH (Figure 2) is analogous to a Cannizzaro reaction (Figure 1), except with $NAD^+$ as the hydride recipient. Assuming, in the enzymatic reaction, that Zn−OH attacks benzaldehyde (eq 5), one might envision benzaldehyde hydrate monoanion oxidation to be involved (Figure 2). A plausible mechanism for such a reaction involves the following: (i) nucleophilic attack of Zn−OH on benzaldehyde bound in the active site of HLADH (as an alternative to binding of the preformed hydrate), (ii) hydride transfer from the *gem*-diol anomeric carbon to C4 of the nicotinamide ring of $NAD^+$, and (iii) proton shuttling from the active site, which might occur either during or after the hydride transfer.

Theoretical approaches have been employed for greater understanding of the reactions of zinc-containing alcohol dehydrogenases. Alcohol−aldehyde redox reactions involving zinc have been studied by *ab initio* (Tapia et al., 1980, 1983, 1991) and semiempirical (von Onciul & Clark, 1993) quantum mechanical methods, but neither approach has been used to study the reactivity of the dehydrogenase as an aldehyde oxidase. The *ab initio* studies by Tapia and coworkers have focused on elucidating the role of zinc, the mechanism by which protons are shuttled from the alcohol substrates in the active site, and transition state geometries. Molecular mechanics and dynamics calculations have recently been performed (Ryde, 1995) on HLADH, in a study which focused on the coordination sphere of zinc when it is bound to water and hydroxide ion.

The original proposal of the formation of a pentacoordinated zinc intermediate (Dworschack & Plapp, 1977) for the replacement of a zinc-bound water with alcoholate anion (eqs 6 and 7), has received little support.

$$[(Cys)_2(His)Zn(OH)]^- + ROH \rightarrow [(Cys)_2(His)Zn(OH_2)(OR)]^- \quad (6)$$

$$[(Cys)_2(His)Zn(OH_2)(OR)]^- \rightarrow [(Cys)_2(His)Zn(OR)]^- + H_2O \quad (7)$$

The X-ray structures of native, as well as metal-depleted, alcohol dehydrogenases indicate a coordination environment with little available space for expansion of the zinc coordination sphere (Eklund et al., 1982). Moreover, AM1 calculations (von Onciul & Clark, 1993) as well as molecular dynamics simulations (Ryde, 1995) suggested that pentacoordinated zinc species should be unfavorable energetically as intermediates in the replacement of zinc-bound water with alcoholate substrate in alcohol dehydrogenase.

In this article, we investigate mechanistic aspects of the oxidation of benzaldehyde, catalyzed by HLADH, using molecular dynamics and semiempirical calculations. X-ray crystal structures are used as templates for structure building, manipulation, and subsequent molecular mechanics and dynamics calculations. To study the assembled dimer, we employ the recently solved X-ray structure for HLADH at 2.1 Å resolution, with pentafluorobenzyl alcohol and $NAD^+$ bound in the active site (Ramaswamy et al., 1994). CHARMM molecular dynamics calculations were employed on assembled reactive ground states [(benzaldehyde hydrate monoanion + $NAD^+$) and (benzaldehyde + zinc/hydroxide + $NAD^+$)], modeled into the active site of alcohol dehy-

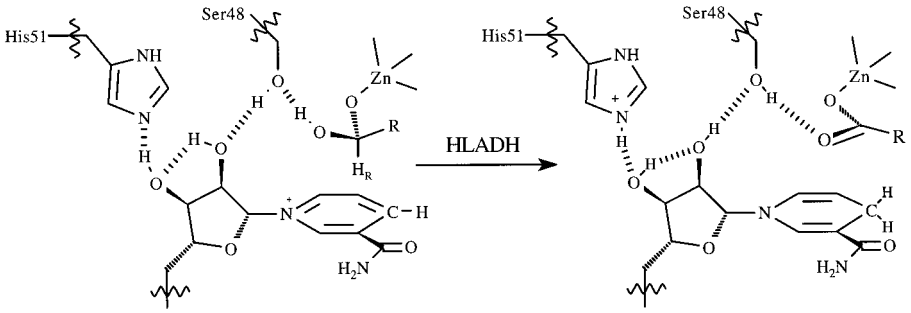


FIGURE 2: Oxidation of an aldehyde hydrate by $NAD^+$ in the active site of horse liver alcohol dehydrogenase. The proton of the aldehyde hydrate is connected by a series of hydrogen bonds to His51 and thence to solvent.

drogenase. Substrates were placed into the active site, using a best-fit superimposition on the pentafluorobenzyl alcohol bound to zinc. Semiempirical PM3 quantum mechanical SCF-MO calculations (Stewart, 1989a,b, 1991) were employed on models of the active site to study aldehyde hydration, hydride transfer, and proton shuttling from the active site. Suggestions regarding the mechanism of aldehyde oxidation catalyzed by HLADH are presented which are based on a combination of molecular dynamics and semiempirical molecular orbital calculations.

## MATERIALS AND METHODS

CHARMM (Brooks et al., 1983) v. 22.5 molecular dynamics simulations were run on a Silicon Graphics workstation. Structural visualization and manipulation of these structures was performed using Quanta, versions 3.3 and 4.0 (MSI, Waltham, MA). Prerelease coordinates for alcohol dehydrogenase with $NAD^+$ and pentafluorobenzyl alcohol at the active site were made available to us by Prof. Bryce Plapp (Ramaswamy et al., 1994). The coordinates of the Brookhaven Protein Data Bank files were modified as follows for dynamic studies. Only polar hydrogens were added to the enzyme structures; extended atoms were used for all carbon chains. The CHARMM residue topology file AMINO.RTF (MSI) was used for the enzyme residues. Water molecules were treated as TIP3P residues (Jorgensen, 1983). The $NAD^+$ cofactor was modified to include all hydrogens. Partial charges for all structures in the RTF were obtained by AM1 calculations. Benzaldehyde and benzaldehyde hydrate monoanion were separately superimposed on pentafluorobenzyl alcohol in the X-ray structures, using the three-dimensional modeling mode of Quanta.

A key feature to be maintained in the molecular dynamics calculations is the geometry of Zn(II) and His67, Cys46, and Cys174 ligands. We have accomplished this by a so-called "bonded approach" of ligand atoms to the zinc, except for the substrate ligands, which were allowed to interact solely via nonbonded potentials. Equilibrium bond lengths as well as angles and dihedral parameters to use for bonding residues His67, Cys46, and Cys174 to Zn(II) were adapted from the parameterization of the zinc ion in HLADH by Ryde (1995). This parameterization is based on *ab initio* calculations of model zinc complexes (Ryde, 1994). The Zn−N(His) (equilibrium bond distance of 2.05 Å) and Zn−$S^-$(Cys) (equilibrium bond distance of 2.30 Å) force constants were set to 300.0 kcal $mol^{-1}$ $Å^{-1}$. It was found that larger force constants and harmonic constraints needed to be applied to the atoms of the active site zinc complex in HLADH in order to ensure structural integrity in the active site during initial energy minimization. After the initial energy minimization of the structure, the larger constraints were released.

Due to the size of the dimer assemblies (>8100 atoms), it was necessary to limit nonbonded interaction calculations by invoking the following constraints. The protein of the A subunit was fixed to the reference (X-ray) set of coordinates. Substrate and cofactor in A were left unconstrained. The entire B subunit was left unconstrained. The assembly was minimized prior to dynamics studies; 100 steps of steepest descents algorithm minimization with a force criterion of 0.001 kcal per 10 steps were followed by the adopted basis Newton−Raphson algorithm for 2000 steps (tolerance of $1 \times 10^{-9}$ kcal per 10 steps). Hydrogen bonds and nonbonding interactions were cut off at 5.0 and 14.0 Å, respectively, and were updated every 25 steps. Dynamics to 100 ps using a time step of 0.001 ps (1000 steps/ps) were run using Verlet integration. Hydrogen bonds were constrained using the SHAKE algorithm (Gunsteren & Berendsen, 1977) during molecular dynamics. The following protocol was used: a heating phase of 3 ps to a final temperature of 300 K, followed by equilibration of 57 ps, and finally 40 ps of observation. Coordinates were saved every 0.05 ps, giving 800 structures from the 40 ps collection phase.

Semiempirical calculations were carried out on model zinc complexes, using the program Ampac 5.0 (Semichem, Inc., 1994) on an SGI Indigo workstation. The PM3 method (Stewart, 1989a,b, 1991) was chosen because it is parameterized for zinc and also has been demonstrated (Jurema & Shields, 1993; Schröder et al., 1991) to more realistically model hydrogen bonds than the AM1 method (Dewar et al., 1985). Calculations were carried out on tetrahedral Zn(II) complexes with $CH_3S^-$ and imidazole; the third and fourth ligands to zinc were either [$CH_3S^-$ + $HO^-$] or [$CH_3S^-$ + PhCH(OH)$O^-$]. All stationary points were fully characterized as such by vibrational analyses. Transition states had only a single imaginary frequency, and ground states had no imaginary frequencies.

## RESULTS

Molecular dynamics simulations were performed on the following assemblies of the dimeric alcohol dehydrogenase: (MD1) enzyme with $NAD^+$, benzaldehyde, and zinc-ligated $HO^-$ in the active site; (MD2) enzyme with $NAD^+$ and with hydrated benzaldehyde monoanion bound to zinc via the *pro-R* oxygen, and the *pro-S* oxygen protonated; and (MD3) enzyme with $NAD^+$ and with hydrated benzaldehyde monoanion bound to zinc via the *pro-S* oxygen, and the *pro-R* oxygen protonated. Preparation for the constructs (MD1−3) is described in Materials and Methods. The molecular dynamics results and statistical analyses are from 800 sample structures taken from the final 40 ps of the 100 ps molecular dynamics simulations. Detailed results of these simulations

Table 1: Zinc−Ligand Distances (Å) from Molecular Dynamics Simulations Utilizing CHARMM Parameters Developed in This Work[a]

| | Zn−(S-CYs420) | Zn−(S-CYs548) | Zn−(N-His441) | Zn−(O-R) |
|---|---|---|---|---|
| MD1 | | | | |
| avg | 2.20 | 2.19 | 2.21 | 1.69[b] |
| SD | 0.004 | 0.004 | 0.004 | 0.020 |
| min | 2.19 | 2.18 | 2.20 | 1.65 |
| max | 2.21 | 2.20 | 2.22 | 1.76 |
| MD2 | | | | |
| avg | 2.34 | 2.35 | 2.08 | 1.93[c] |
| SD | 0.025 | 0.026 | 0.028 | 0.037 |
| min | 2.27 | 2.28 | 2.01 | 1.85 |
| max | 2.40 | 2.42 | 2.15 | 2.02 |
| MD3 | | | | |
| avg | 2.20 | 2.20 | 2.21 | 1.92[c] |
| SD | 0.0001 | 0.0001 | 0.0003 | 0.037 |
| min | 2.20 | 2.20 | 2.21 | 1.84 |
| max | 2.20 | 2.20 | 2.21 | 2.06 |

[a] Zinc−heteroatom distances. [b] Zinc−oxygen distance; R = H. [c] Zinc−oxygen distance; R = CH(OH)Ph.

Table 2: $NAD^+$ $X_{am}$ and $X_n$ Angle Parameters from MD1−3[a]

| | $X_{am}$ | $X_n$ |
|---|---|---|
| MD1 | | |
| avg | −162.3 | −125.1 |
| min | −178.6 | −157.2 |
| max | −144.8 | −92.1 |
| MD2 | | |
| avg | −159.1 | −115.7 |
| min | −179.4 | −138.4 |
| max | −139.2 | −92.2 |
| MD3 | | |
| avg | −149.5 | −97.5 |
| min | −174.0 | −111.0 |
| max | −127.8 | −83.9 |

[a] See Figure 3 for definition angles.

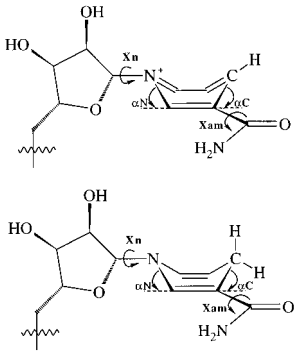


FIGURE 3: $NAD^+$ conformational angle parameters. Positive and negative values are defined with respect to the orientation shown here. For positive values of $X_{am}$ (C2−C3−C═O dihedral angle), the carbonyl oxygen points upward, and a negative value of $X_n$ (ribose O−ribose C1−nicotinamide N1−nicotinamide C2) has the ribose ether oxygen below the ring, as shown. Both $\alpha_C$ and $\alpha_N$ are positive if the ring is bent upward (as shown) and are negative if the ring is bent downwards.

are presented in the following sections along with the related semiempirical calculations.

Table 1 lists distances about the active site zinc from the three molecular dynamics simulations (MD1−3). The stability of the zinc complexes in the active site is evident. Table 2 lists selected geometrical parameters of the $NAD^+$ cofactor in these simulations. The significance of the angles $X_n$ and $X_{am}$ (Figure 3) has been discussed elsewhere [see Almarsson and Bruice (1993); Wu and Houk (1991, 1993), and Wu et al. (1995) and references therein] in terms of their effects on energetics of hydride transfer. We merely point out here that computations in the aforementioned references suggest that $X_n$ near ±90° destabilizes $NAD^+$ relative to NADH, by a stereoelectronic effect caused by the ribose ether oxygen's geometry relative to the nicotinamide ring. Computations also show that an $X_{am}$ of ∼180° has a surprisingly potent energy-lowering effect on the transition state for hydride transfer relative to the situation when $X_{am}$ is ∼0°. This effect of $X_{am}$ is still not fully understood. The ring-puckering angles $\alpha_C$ and $\alpha_N$ (Raber & Rodriguez, 1985; Wu & Houk, 1991, 1993; Almarsson & Bruice, 1993; Wu et al., 1995) are important in hydride-transfer reactivity but are small in the case of the oxidized cofactor in this work, so are not reported for the molecular dynamics part of this study.

*Hydration of Benzaldehyde in the HLADH Active Site.* The purpose of running the simulation with benzaldehyde and hydroxide ion bound to zinc at the active site (MD1) was to determine whether HLADH might catalyze hydration of the aldehyde, as the hydrate is required for its subsequent oxidation to carboxylate. The dynamics simulation reveals (Figures 4 and 5) that the zinc hydroxyl oxygen is in close association (average distance of 3.7 ± 0.64$\sigma$ Å) with the carbonyl carbon of benzaldehyde. The distance ranged from 2.8 to 5.5 Å, with the Zn−O−C angle of 142.3° ± 16.6$\sigma$ (where the oxygen is the zinc-bound hydroxide oxygen and the carbon is the benzaldehyde carbonyl carbon).

For semiempirical calculations of the aldehyde hydration process, the model system used was the complex $[(CH_3S^-)_2$-(Im)Zn−OH$]^-$ (Table 3; RCT, Figure 6) and benzaldehyde. The first step in the pathway is nucleophilic attack of the zinc-ligated hydroxide oxygen on benzaldehyde carbonyl carbon. The transition state (TS1, Figure 6) for this reaction is 6.6 kcal/mol higher in enthalpy than the infinitely separated reactants. The Zn−O−C angle in this transition state (131.3°) is within one standard deviation of the average Zn−O−C angle calculated during molecular dynamics, and the O−C distance (1.877 Å) is only ∼0.9 Å closer than the closest approach seen in 40 ps of dynamics sampling. The intermediate (INT, Figure 6) is calculated to be lower in enthalpy than the reactants by 0.1 kcal/mol. This zwitterionic form is not the most stable arrangement, compared to having the oxyanion ligated to zinc. Two transition states which achieve such a rearrangement were computed, differing in whether the zinc ion or the proton migrates to the oxyanion. Zinc migrates via a pentacoordinate transition state (TS2a, Figure 6) which is 8.6 kcal/mol higher in enthalpy than the infinitely separated reactants. Alternatively, migration of a proton gives a transition state (TS2b, Figure 6) which is 27.7 kcal/mol higher in enthalpy than the infinitely separated reactants. Proton-transfer transition state energies may be greatly overestimated by PM3 (Zheng et al., 1993; Ríos & Rodríguez, 1992), so TS2b may in fact be competitive with TS2a. The product (PROD, Figure 6) of whichever rearrangement (TS2a or TS2b) that results in binding of the oxyanion to zinc is calculated to be 7.1 kcal/mol lower in enthalpy than the reactants.

An interesting feature of the PM3 structures is that they reveal an apparently strong interaction (<1.8 Å H−O distances listed in Table 3) between the hydrogen attached to C2 of imidazole and the oxygen which is bonded either to zinc (RCT, Figure 6), to benzaldehyde hydrate (TS1, INT, and TS2b, Figure 6), or to both zinc and benzaldehyde hydrate (TS2a and PROD, Figure 6). Coincidentally, we have recently observed similar interactions, using *ab initio* calculations, between imidazole C2 hydrogens and amide

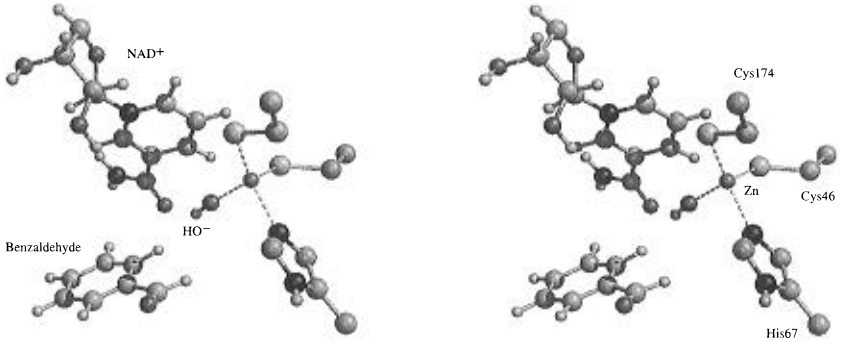


FIGURE 4: Stereoview of a representative instantaneous molecular dynamics structure of the active site of the HLADH complex with $NAD^+$, benzaldehyde, and zinc-bound hydroxide ion at the active site (MD1). The Zn−O−C angle formed by zinc, the hydroxide oxygen, and the carbonyl carbon was 142.3 ± 16.6$\sigma$° during the simulation.

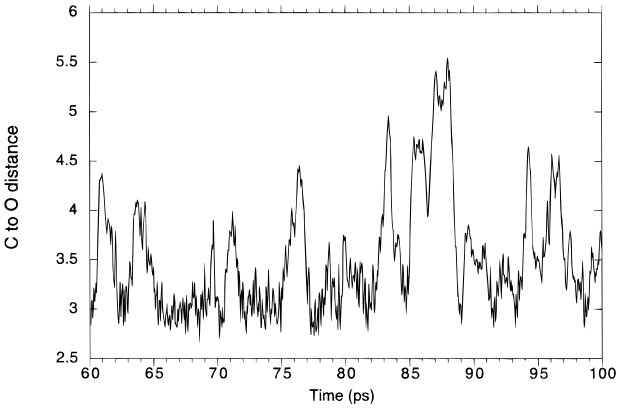


FIGURE 5: Plot of the distance between the benzaldehyde α-carbon and the oxygen ligated to zinc during the sampling phase (800 structures) of 40 ps in the MD1 simulation. The oxygen of the zinc-ligated $HO^-$ had a mean distance of 3.7 ± 0.64$\sigma$ Å (range, 2.8−5.5 Å) from the carbonyl carbon of benzaldehyde.

carbonyl oxygens (Olson & Bruice, 1995). We interpret this type of interaction as a hydrogen bond, in agreement with the recent analyses by Derewenda et al. (1994, 1995) of such interactions in X-ray crystal structures of proteins. It has been shown [see Clement et al. (1996) for recent results and discussion] that imidazole ligation to metal ions increases the lability to base of the imidazole C2 hydrogen, thus further supporting the interpretation that this acidic hydrogen can form hydrogen bonds.

An exhaustive analysis of pathways for exchange of water for alcohols and aldehydes as ligands to zinc in the active site of HLADH is beyond the scope of this paper; however, some attempts were made to model the process of binding of an already-formed aldehyde hydrate to zinc, using PM3. Approach of the hydrate oxygen to zinc in either zinc/hydroxide or zinc/water complexes resulted only in monotonic increases in energy as the complex went from four to five coordination of Zn(II). It was also found that neutral hydrates $RCH(OH)_2$ did not remain bound to $[(CH_3S)_2$-(imidazole)Zn] or to $[(CH_3SH)(CH_3S)$(imidazole)$Zn]^+$. Rather, the neutral hydrate was ejected, and a trigonal-planar complex of Zn(II) attached to thiol(ate) and imidazole ligands formed. If, however, hydrate monoanion $RCH(OH)O^-$ was bound to zinc via the anionic oxygen, a tetrahedral Zn(II) complex was stable, regardless of whether an overall charge of 0 (corresponding to one thiol and one thiolate ligand) or −1 (corresponding to two thiolate ligands) resided on the complex.

*Hydride Transfer from the Aldehyde Hydrate to $NAD^+$.* Two dynamics simulations were done to study the stereochemical details of HLADH catalysis of hydride transfer from benzaldehyde hydrate to $NAD^+$. The starting configurations were created by minimal perturbation of the zinc-bound $C_6F_5CH_2O^-$ in the X-ray structure by replacement by best-fit superimposition with $C_6H_5CH(OH)O^-$ to give *R* and *S* isomers of zinc-bound benzaldehyde hydrate monoanion. The resulting configurations were then used for molecular dynamics (MD2 and MD3).

Simulation MD2 was done with the *pro-S* oxygen protonated, and the *pro-R* oxygen ligated to zinc (Figure 7). The

Table 3: Enthalpies and Selected Geometrical Parameters for PM3-Computed Ground State and Transition State Models for Benzaldehyde Hydration by $[(HO)Zn(CH_3S)_2(Im)]^-$

| | reactants[a] | TS1 | intermediate | TS2a | TS2b | product |
|---|---|---|---|---|---|---|
| $\Delta H_f$ (kcal/mol) | −10.65 (PhCHO)<br>−100.06 ($ZnL_4$) | −104.07 | −110.79 | −102.13 | −83.03 | −117.75 |
| $i$ ($cm^{-1}$) | − | −256.8 | − | −114.3 | −2421.0 | − |
| Zn−O1[b] (Å) | 1.970 | 2.103 | 2.329 | 2.468 | 2.098 | 3.904 |
| Zn−O2[c] (Å) | − | 4.027 | 3.755 | 2.803 | 3.562 | 2.123 |
| Zn−S1[d] (Å) | 2.375 | 2.355 | 2.327 | 2.347 | 2.355 | 2.354 |
| Zn−S2[e] (Å) | 2.380 | 2.343 | 2.320 | 2.333 | 2.345 | 2.347 |
| Zn−N (Å) | 2.104 | 2.082 | 2.040 | 2.057 | 2.084 | 2.101 |
| O−C[f] (Å) | − | 1.877 | − | − | − | − |
| Im(H)−O[g] (Å) | − | 1.756 | 1.658 | 1.672 | 1.729 | 1.780 |
| Im(C−H)−O[h] (deg) | − | 173.0 | 165.0 | 141.3 | 156.0 | 130.2 |
| ∠Zn−O−C[i] (deg) | − | 131.3 | − | − | − | − |
| ∠O−Zn−O[j] (deg) | − | − | − | 46.7 | − | − |
| ∠O−H−O[k] (deg) | − | − | − | − | 102.5 | − |

[a] At infinite separation. [b] Oxygen originally attached to Zn. [c] Oxygen originally from PhCHO. [d] *pro-R* sulfur. [e] *pro-S* sulfur. [f] TS1 carbonyl attack distance. [g] H−O distance from C−H−O hydrogen bond. [h] Angle of C−H−O hydrogen bond. [i] TS1 carbonyl attack angle. [j] TS2a Zn migration angle. [k] TS2b $H^+$ migration angle.

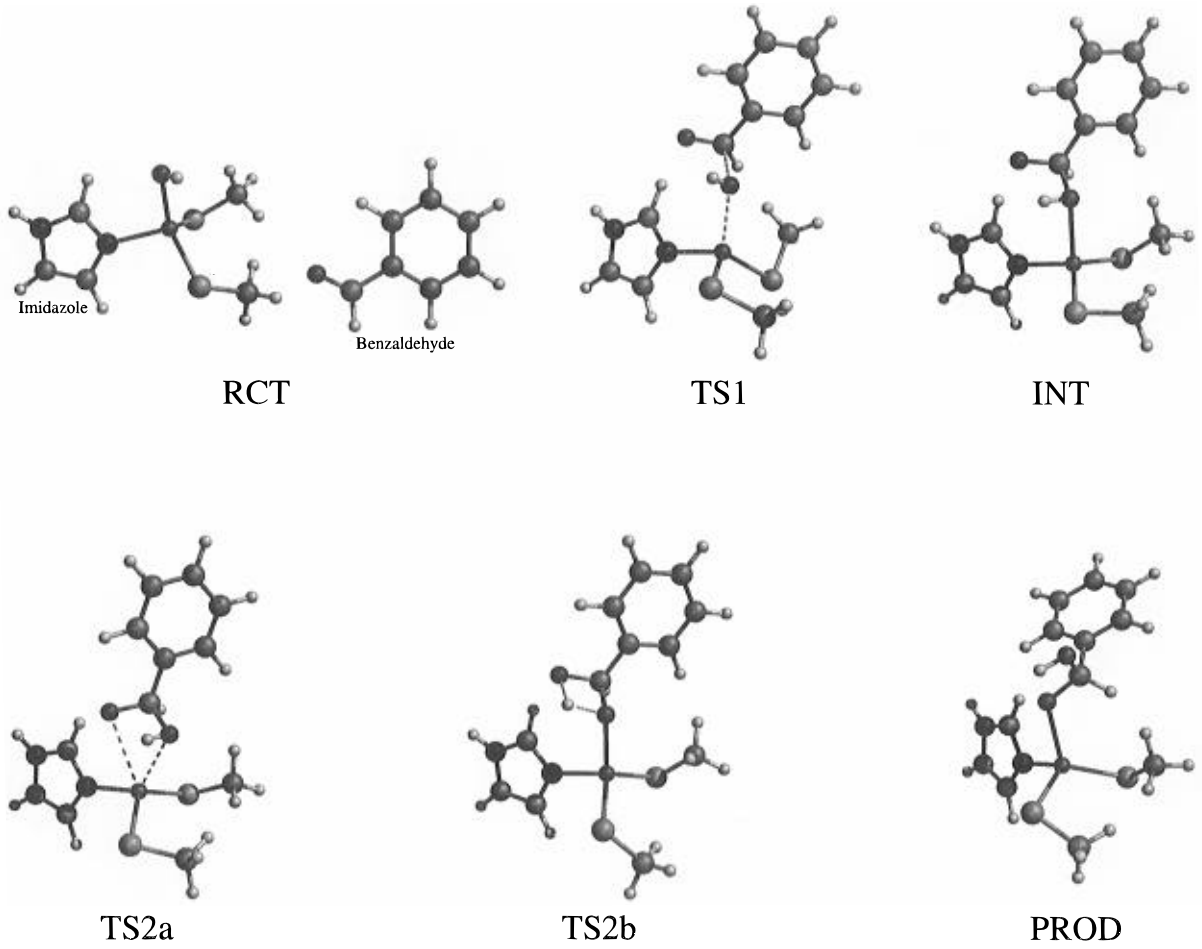


FIGURE 6: PM3-computed ground states and transition states of a model system for aldehyde hydration by HLADH: RCT, structures of benzaldehyde and of zinc ligated to imidazole, hydroxide, and two thiolates; TS1, transition state for nucleophilic attack of the zinc-ligated hydroxide oxygen on benzaldehyde carbonyl carbon; INT, structure of the intermediate with zinc and a proton attached to the same oxygen (the former carbonyl oxygen is present as the oxyanion); TS2a, transition state for exchange of the zinc−oxygen bond from the neutral oxygen of the benzaldehyde hydrate monoanion to the oxyanionic oxygen; TS2b, transition state for migration of a proton to the oxyanion; PROD, structure of hydrated benzaldehyde ligated to zinc via the oxyanion. Table 3 lists enthalpies and selected geometric parameters for these molecules.

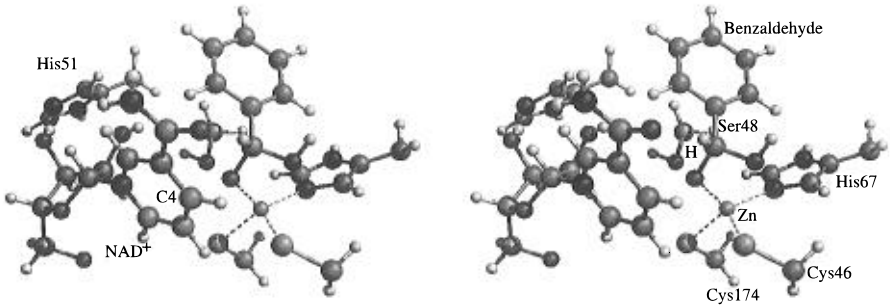


FIGURE 7: Stereoview of a representative instantaneous molecular dynamics structure of the active site of the HLADH complex with $NAD^+$ and the benzaldehyde hydrate monoanion (MD2). The hydrate *pro-S* oxygen is protonated, and the *pro-R* oxygen is ligated to Zn(II). The *pro-S* oxygen varied between 2.9 and 3.9 Å (average, 3.5 Å) from zinc. The proton on the *pro-S* oxygen was on average 3.9 Å from the hydroxyl oxygen of Ser48.

benzylic hydrogen was 2.79 ± 0.13$\sigma$ Å from C4 of $NAD^+$. The C−H−C angle (formed by C4 of $NAD^+$, the hydride, and the benzaldehyde α-carbon) was 132.9° ± 5.9$\sigma$. However, Ser48, which is believed to assist in proton transfer from the active site (Eklund et al., 1982) to the external environment, does not interact with the free hydrogen on the benzaldehyde hydrate (H−O distance of 3.9 ± 0.14$\sigma$ Å).

The simulation with the *pro-S* oxygen ligated to zinc and the *pro-R* oxygen protonated (MD3) provided a geometry somewhat more favorable for hydride transfer (Figure 8). The aldehyde hydrate benzylic hydrogen to $NAD^+$ C4 distance (2.56 ± 0.12$\sigma$ Å) was slightly closer than that in MD2 (Figure 9). The C−H−C angle (137.8° ± 11.2$\sigma$) was slightly closer in MD3 to that in the PM3-calculated transition state for hydride transfer (Table 4).[2] The hydrogen on the *pro-R* oxygen was only 2.09 ± 0.19$\sigma$ Å from the hydroxyl oxygen of Ser48. Thus, Ser48 is poised to assist with proton shuttling from the active site in the structure generated from MD3.

The active site geometry used in MD3 was used as a starting point for PM3 calculations of a model system for

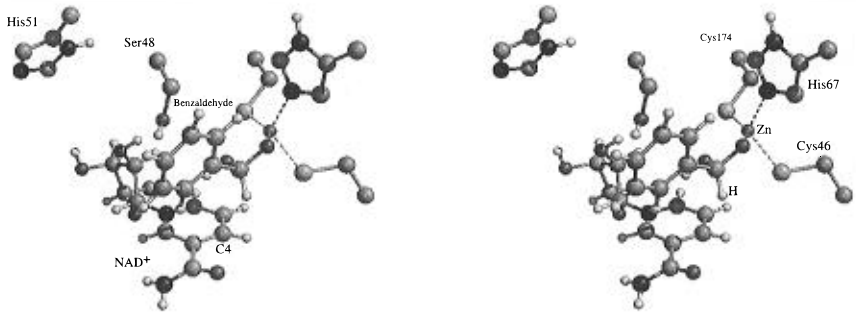


FIGURE 8: Stereoview of a representative instantaneous molecular dynamics structure of the active site of the HLADH complex with $NAD^+$ and the benzaldehyde hydrate monoanion (MD3). The *pro-R* oxygen is protonated, and the *pro-S* oxygen is ligated to Zn(II). The *pro-R* oxygen varied between 3.0 and 3.5 Å (average, 3.2 Å) from zinc. The hydrogen on the *pro-R* oxygen was on average 2.1 Å from the hydroxyl oxygen of Ser48.

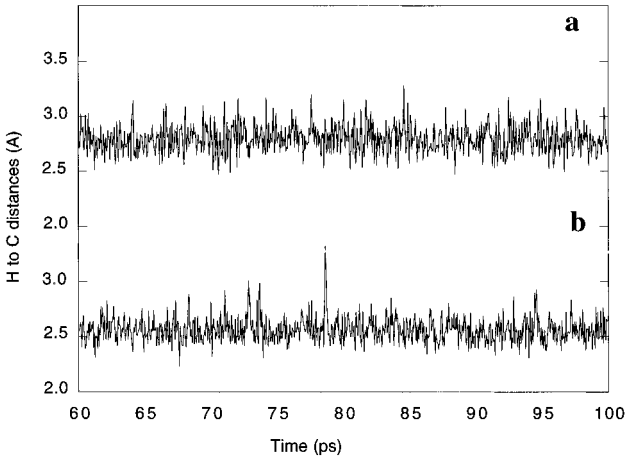


FIGURE 9: Comparison of distances of hydrogen attached to the benzaldehyde hydrate α-carbon from $NAD^+$ C4 in two simulations. In MD2 (9a), this distance was $2.79 \pm 0.13\sigma$ Å; in MD3 (9b), this distance was $2.56 \pm 0.12\sigma$ Å. Data are from 800 sample structures from each run taken from the 40 ps sampling phase.

hydride transfer.[2] Reactants were placed in positions that overlapped the corresponding atoms of MD3. The system used was *N*-ribosyl nicotinamide ($NAD^+$ mimic), connected solely via hydrogen bonds to imidazole (His51 mimic) and methanol (Ser48 mimic) by the ribose 3′- and 2′-OH groups; the methanol, in turn, was hydrogen-bonded to the *pro-R* hydroxyl proton of benzaldehyde hydrate monoanion, and finally, the *pro-S* oxygen of benzaldehyde hydrate monoanion was ligated to $[Zn(CH_3SH)(CH_3S)(Im)]^+$. It was found after a subsequent complete PM3 geometry optimization that the series of hydrogen bonds was sufficient to hold the zinc-bound substrate and the nicotinamide cofactor in close proximity, with no artificially introduced constraints (Figure 10a). The transition state for hydride transfer was also located (Figure 10b) and was computed to be 21.5 kcal/mol higher in enthalpy than the reactants. Finally, the geometry and enthalpy of the products were calculated (Figure 10c); hydride transfer was exothermic by 23.5 kcal/mol.

[2] A set of simulations was also performed with a more rigid model of the active site. This model used manually adjusted parameters to maintain relatively strict correlation of the Zn(II)-coordinating ligands (His67, Cys46, and Cys174) with their X-ray crystal structure geometry during dynamics. Using these alternative parameters, there was a more clear-cut preference for the MD3 hydride transfer angles and distances over MD2. The C−H−C angle and C−H distance averages were 86.8° and 3.95 Å (MD2) vs 137.8° and 2.56 Å (MD3), respectively. In all other respects, the simulations with either the manually adjusted zinc parameters or the zinc parameters of Ryde (1995) were virtually identical.

Table 4: Enthalpies and Selected Geometrical Parameters for the PM3-Computed Ground State and Transition States for Models of Hydride Transfer to $NAD^+$

| molecule | $NAD^+$/aldehyde hydrate model (Figure 10a) | hydride transfer transition state (Figure 10b) | NADH/benzoic acid model (Figure 10c) |
|---|---|---|---|
| $\Delta H_f$ (kcal/mol) | −137.4 | −115.9 | −160.9 |
| $i$ ($cm^{-1}$) | − | −1588.0 | − |
| $C_b-H_t$[a] (Å) | 1.122 | 1.433 | 3.950 |
| $C4-H_t$[b] (Å) | 3.265 | 1.476 | 1.118 |
| ∠Cb−$H_t$−C4 (deg) | 131.2 | 171.7 | 133.1 |
| $X_{am}$[c] (deg) | 128.3 | −163.1 | 126.7 |
| $X_n$[c] (deg) | −116.8 | −113.2 | −89.9 |
| $\alpha_C$[c] (deg) | 2.4 | 8.8 | 11.2 |
| $\alpha_N$[c] (deg) | 2.7 | 5.8 | 11.7 |

[a] $C_b$ = benzaldehyde or benzoic acid α-carbon; Ht = transferring hydrogen. [b] C4 = nicotinamide or dihydronicotinamide C4. [c] See Figure 3 for definition.

The C4−H distance in the PM3 transition state was a mere 0.85 Å closer than that in a structure observed in only 40 ps of molecular dynamics sampling. The transition state C−H−C angle was only 35° closer to linearity than the average geometry in the molecular dynamics simulations. Comparison of molecular dynamics and semiempirical results suggests that very little additional motion beyond that observed in the ground state MD3 simulations should be required to achieve hydride transfer from aldehyde hydrate to $NAD^+$.

*Proton Shuttling from the Active Site of HLADH.* As mentioned earlier, a series of hydrogen bonds is thought to provide a channel through which the proton can be carried out of the active site or removed from the hydrate either during or after catalysis (Tapia et al., 1980, 1983, 1991; Eklund et al., 1982; von Onciul & Clark, 1993).

In 40 ps of sampling from the simulation MD3 (Figure 8), the proton attached to the *pro-R* oxygen formed a hydrogen bond ($2.09 \pm 0.19\sigma$ Å; range of 1.70−2.69 Å) with the Ser48 hydroxyl oxygen. The Ser48 hydroxyl proton, however, "flipped" before the sampling phase; thereafter, it was only intermittently hydrogen-bonded to the $NAD^+$ ribose 2′-hydroxyl oxygen ($3.25 \pm 0.13\sigma$ Å; range of 3.0−3.6 Å). Likewise, the ribose 2′-hydroxyl proton interacted only weakly with the 3′-hydroxyl oxygen ($3.42 \pm 0.10\sigma$ Å; range of 3.2−3.7 Å) during the sampling phase; thereafter, this proton was hydrogen-bonded to Ser48 oxygen ($2.16 \pm 0.16\sigma$ Å; range of 1.83−2.90 Å). The ribose 3′-hydroxyl proton hydrogen bonded to both His51 nitrogen ($2.34 \pm 0.29(\sigma)$ Å; range 1.9−3.3Å) and ribose 2′-hydroxyl oxygen ($2.10 \pm 0.16\sigma$ Å; range of 1.8−2.5 Å). It is probable that the enzyme in its dynamic motions would from time to

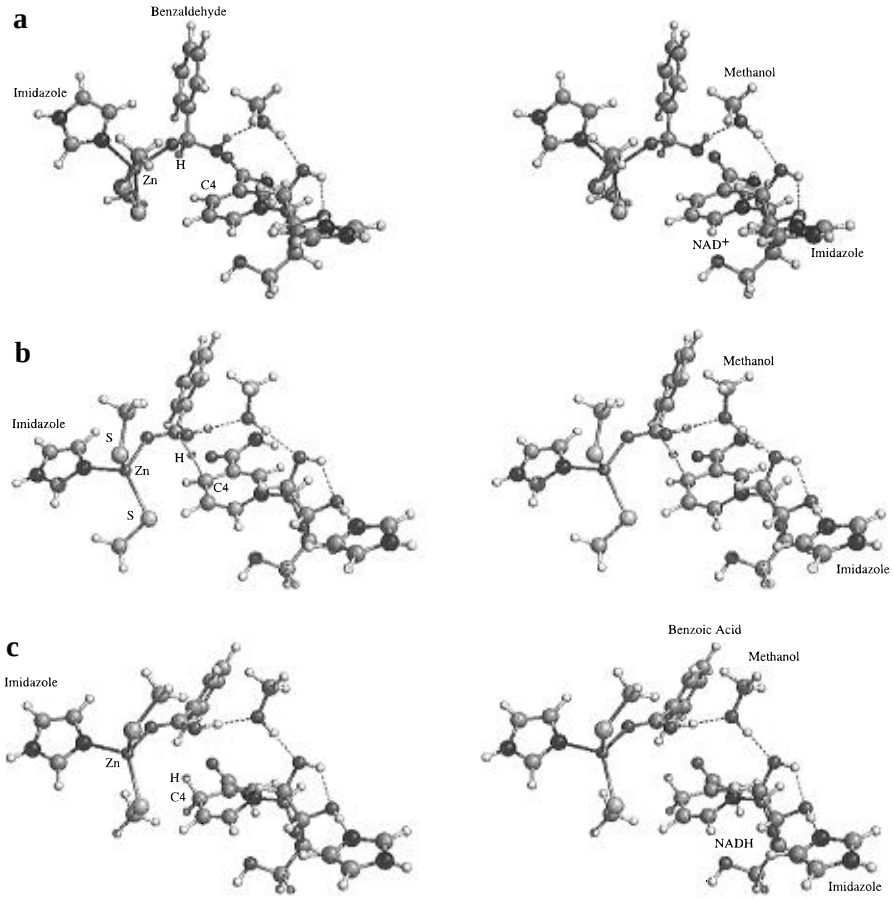


FIGURE 10: PM3-calculated ground states and transition states for models of hydride transfer from the benzaldehyde hydrate carbon to C4 of $NAD^+$: (a) reactants (zinc-ligated benzaldehyde hydrate and *N*-ribosyl nicotinamide hydrogen-bonded to methanol and imidazole), (b) hydride transfer transition state, and (c) products (zinc-ligated benzoic acid and *N*-ribosyl dihydronicotinamide hydrogen-bonded to methanol and imidazole). Enthalpies and selected geometrical parameters for these molecules are listed in Table 4.

time display a proton arrangement which would complete the proton-shuttling system, such that the Ser48 proton would flip back to hydrogen bond with the 2′-hydroxyl oxygen, while the 2′-hydroxyl proton would flip back to hydrogen bond with the 3′-hydroxyl oxygen.

In the PM3 hydride-transfer calculations, the proton on the developing benzoic acid was strongly hydrogen-bonded to $CH_3OH$ (Ser48 mimic) during hydride transfer, but no simultaneous proton transfer occurred. Nonetheless, it seemed reasonable to investigate further whether the shuttle system might operate by a concerted series of proton transfers after hydride transfer. The starting point for PM3 calculations of proton shuttling was the product (Figure 10c) of the hydride-transfer reaction. It was found using this system that proton shuttling was not concerted; i.e., at no point did moving one proton induce a barrierless series of proton transfers. Rather, four discrete steps were required, with three protonated alcohol intermediates in the pathway (Figure 11). To achieve net proton transfer from benzoic acid in the reactant ($\Delta H_f = -160.9$ kcal/mol) to imidazole in the product, it was necessary to move (i) the benzoic acid proton to $CH_3OH$ oxygen ($\Delta H_f$ of the intermediate $= -131.7$ kcal/mol), (ii) the original $CH_3OH$ hydroxyl proton to ribose 2′-hydroxyl oxygen ($\Delta H_f$ of the intermediate $= -125.5$ kcal/mol), (iii) the original ribose 2′-hydroxyl proton to ribose 3′-hydroxyl oxygen ($\Delta H_f$ of the intermediate $= -129.2$ kcal/mol), and (iv) the original ribose 3′-hydroxyl proton to imidazole nitrogen ($\Delta H_f$ of the product $= -163.7$ kcal/mol).

Since proton transfer barrier heights are known to be substantially overestimated by the PM3 method (Zheng et al., 1993; Ríos & Rodríguez, 1992), no formal transition states were computed for these processes. However, all of the reactants, intermediates, and products were characterized as local minima by frequency calculations (Figure 11). Net proton transfer from benzoic acid to imidazole was computed to be exothermic by 2.8 kcal/mol, so there is a driving force for proton shuttling. However, the intermediates in this pathway are as much as 35.4 kcal/mol higher in enthalpy than the reactants (Figure 10c). Of course, the enthalpies of the polar intermediates and product were computed in the gas phase and may be overestimated with respect to the relatively nonpolar reactants.

## DISCUSSION

*HLADH-Catalyzed Hydration of Benzaldehyde.* Our calculations suggest that it is possible that HLADH could catalyze hydration of an aldehyde when hydroxide is ligated to the active site zinc. Molecular dynamics results suggest that the geometry is favorable for nucleophilic attack of zinc-bound hydroxide ion on the aldehyde carbonyl carbon. When the aldehyde carbon to hydroxyl oxygen distances in the ground state simulation are compared to those of the PM3 transition state for hydration, it is apparent that very little motion (~0.85 Å closer approach) in addition to that observed in the dynamics simulation should be required for hydration of the aldehyde. The enthalpy barriers to hydration of benzaldehyde by Zn−OH (6.6 kcal/mol for carbonyl attack and 8.6 kcal/mol for zinc migration) seem low enough to be easily overcome, unless the barrier heights are drastically underestimated by PM3. Thus HLADH-catalyzed hydration

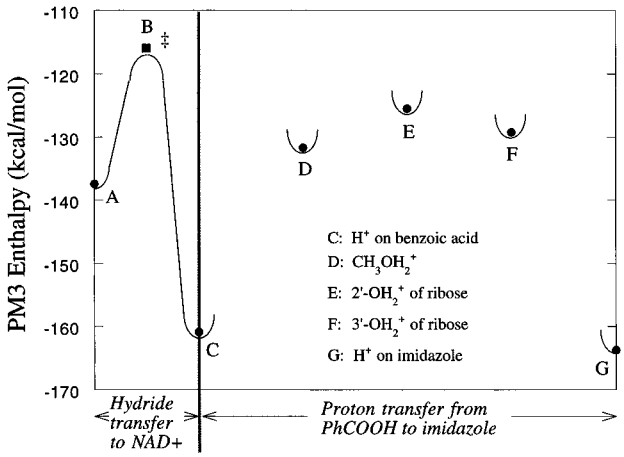


FIGURE 11: Diagram of PM3-calculated enthalpies of the model system for hydride transfer and proton shuttling. Points A−C correspond to the hydride transfer pathway structures (Figure 10a−c). Points D−G are potential energy minima for net proton transfer from benzoic acid to imidazole in this model system. The heavy atom locations for points D−G are essentially those of point C (Figure 10c); they differ primarily in the location of the protons in the shuttle pathway (depicted schematically in Figure 2). Semiempirical methods do not accurately characterize proton transfer barrier heights, so the saddle points in the trajectories connecting points C and D, D and E, E and F, and F and G were not explicitly located. However, all of the labeled points are stationary points on the PM3 potential energy surface, proven by vibrational frequency analyses. The presence of three distinct minima (points D−F) in the proton-shuttling pathway argues against a simultaneous hydride transfer/proton shuttling mechanism, even though partial deprotonation of the zinc-bound hydrate might be expected to facilitate hydride transfer.

of aldehydes is a likely alternative to binding of minute mole fractions of preformed hydrate.

We found no pentacoordinate zinc species corresponding to local energy minima which were formed in hydration of aldehydes. The calculations suggesting accessibility of three-coordinate zinc may be compared to the X-ray crystallographic results of Gruff and Koch (1989), in which the complex tris[(2,3,5,6-tetramethylphenyl)thiolato]zinc(II)$^-$ was found to exist in a trigonal-planar configuration about zinc (despite crystallization from acetonitrile). This was a surprising result, in that those authors had considered a more likely outcome to be coordination of a molecule of solvent to form a tetrahedral complex. Indeed, they found that reaction of the trigonal-planar $[Zn(SR)_3]^-$ complex with 1-methylimidazole (a more avid ligand for zinc than acetonitrile) resulted in formation of a four-coordinate complex $[Zn(SR)_3(1\text{-Me-Im})]^-$. By analogy, alkoxides (including aldehyde hydrate monoanions) should be more avidly coordinating ligands for zinc than the corresponding alcohols or aldehyde hydrates. It may not be entirely unreasonable for neutral alcohols and aldehyde hydrates to spontaneously dissociate from zinc to give an intermediate three-coordinate $[Zn(SR)_2(Im)]$ complex.

This raises the possibility of three-coordinate zinc as an intermediate in the active site of the enzyme, as a means of exchanging water and alcohol (or aldehyde hydrate) ligands (eqs 8 and 9). This has potential implications for the alcohol

$$(Cys)_2(His)Zn-OH + H^+ \rightarrow (Cys)_2(His)Zn + H_2O \quad (8)$$

$$(Cys)_2(His)Zn + ROH \rightarrow (Cys)_2(His)Zn-OR + H^+ \quad (9)$$

dehydrogenase reactivity of HLADH, as was also suggested

Chart 1

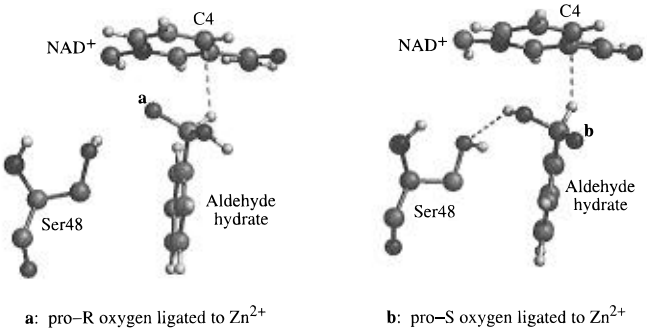


**a**: pro−R oxygen ligated to $Zn^{2+}$ **b**: pro−S oxygen ligated to $Zn^{2+}$

by Ryde (1995). This was also suggested in general for enzymes containing zinc ligated to cysteines by Gruff and Koch (1989). Full consideration of mechanisms for association and dissociation of ligands to and from Zn(II) in HLADH is beyond the scope of this paper, but further studies would undoubtedly be of considerable interest.

*Geometry of Hydride Transfer from Hydrate to NAD* . The $NAD^+$ C4 to aldehyde hydrate C−H is somewhat more favorable for hydride transfer when the *pro-S* oxygen, as compared to the *pro-R* oxygen, is ligated to zinc (Figures 7 and 8). The structures of Chart 1, created from Figures 7 and 8, show that ligation of *pro-S* oxygen of benzaldehyde hydrate at a $Zn^{2+}$ allows hydrogen bonding to Ser48. Aside from this hydrogen bond allowing proton shuttling away from the benzoic acid product, it may provide a stabilization of the structure which is not apparent when the *pro-R* oxygen is ligated to $Zn^{2+}$.

The proximity of reactants in simulations MD2 and MD3 is striking. Very little additional motion aside from ground state dynamic motion is required to achieve hydride transfer. One might be concerned that the PM3 calculations do not adequately model the transition state (Figure 10b) compared to high-level *ab initio* calculations. However, the PM3 geometry and activation enthalpy for hydride transfer in this system agree reasonably well with *ab initio* values for related hydride transfers (Wu & Houk, 1991, 1993; Wu et al., 1995). Furthermore, in contrast to proton-transfer transition states, which are poorly represented by semiempirical methods (Zheng et al., 1993; Ríos & Rodríguez, 1992), hydride transfers are fairly well-represented (Cummins & Gready, 1989, 1990; Zheng et al., 1993; Andrés et al., 1995). Nonetheless, *ab initio* calculations of reduction of $NAD^+$ by zinc-bound aldehyde hydrate seem warranted.

*Proton Shuttling from the Active Site of HLADH.* Our calculations support the possibility of shuttling of protons out of the active site (Eklund et al., 1982) by the series of hydrogen bonds depicted in Figure 2. However, proton shuttling through this series of donors and acceptors did not appear to be coupled with hydride transfer from the hydrate. Rather, three discrete intermediates were located in a pathway which accomplishes proton shuttling from the benzoic acid product to the imidazole. Although this seems to be an exothermic process, it appears that such a shuttle provides little direct benefit to catalysis of hydride transfer in the case of aldehyde oxidation. Not only are hydride transfer and proton transfer entirely separate reactions, but no anomalously strong (i.e., shortened) hydrogen bonds are observed in the PM3 hydride-transfer transition state (Figure 10b) when compared to the ground state (Figure 10a). This is consistent with kinetic studies which suggest that, in the

alcohol dehydrogenase reaction of HLADH, proton transfer and hydride transfer are not coupled (Klinman, 1981).

During the sampling phase of the molecular dynamics simulation MD3, there was an incomplete shuttle relative to that depicted in Figure 2. This was because Ser48 acted as a hydrogen bond acceptor to both the aldehyde hydrate and the 2′-hydroxyl group during most of the 40 ps sampling phase. The Ser48 proton can easily donate to the ribose 2′-hydroxyl oxygen, and likewise, the ribose 2′-hydroxyl proton can easily donate to the 3′-hydroxyl oxygen, thereby achieving the most desirable hydrogen-bonding configuration for proton shuttling.

## ACKNOWLEDGMENT

We thank Professor Bryce V. Plapp for early access to the 2.1 Å resolution crystal structure of the HLADH/$NAD^+$/pentafluorobenzyl alcohol complex. We acknowledge the kind assistance of Felice Chu and Helgi Adalsteinsson with several figures.

## REFERENCES

Abeles, R. H., & Lee, H. A., Jr. (1960) *J. Biol. Chem. 235*, 1499−1503.
Almarsson, Ö., & Bruice, T. C. (1993) *J. Am. Chem. Soc. 115*, 2125−2138.
Andrés, J., Safont, V. S., Martins, J. B. L., Beltrán, A., & Moliner, V. (1995) *THEOCHEM 330*, 411−416.
Bahnson, B. J., Park, D.-H., Kim, K., Plapp, B. V., & Klinman, J. P. (1993) *Biochemistry 32*, 5503−5507.
Bowden, K., El Kaissi, F. A., & Ranson, R. (1990) *J. Chem. Soc., Perkin Trans. 2*, 2089−2097.
Brändén, C. I., Jörnvall, H., Eklund, H., & Furugren, B. (1975) *The Enzymes* (Boyer, P. D., Ed.) 3rd ed., Vol. 11, p 103, Academic Press, New York.
Brooks, B. R., Bruccoleri, R. E., Olafson, B. D., States, D. J., Swaminathan, S., & Karplus, M. (1983) *J. Comput. Chem. 4*, 187−217.
Clement, O., Roszak, A. W., & Buncel, E. (1996) *J. Am. Chem. Soc. 118*, 612−620.
Corwin, D. T., Jr., & Koch, S. A. (1988) *Inorg. Chem. 27*, 493−496.
Cummins, P. L., & Gready, J. E. (1989) *THEOCHEM 183*, 161−174.
Cummins, P. L., & Gready, J. E. (1990) *J. Comput. Chem. 11*, 791−804.
Dalziel, K., & Dickinson, F. M. (1965) *Nature 206*, 255−257.
Derewenda, Z. S., Derewenda, U., & Kobos, P. M. (1994) *J. Mol. Biol. 241*, 83−93.
Derewenda, Z. S., Lee, L., & Derewenda, U. (1995) *J. Mol. Biol. 252*, 248−262.
Dewar, M. J. S., Zoebisch, E. G., Healy, E., & Stewart, J. J. P. (1985) *J. Am. Chem. Soc. 107*, 3902−3909.
Dworschack, R. T., & Plapp, B. V. (1977) *Biochemistry 16*, 2716−2725.
Eisses, K. T. (1989) *Bioorg. Chem. 17*, 268−274.
Eklund, H., Plapp, B. V., Samama, J.-P., & Brändén, C.-I. (1982) *J. Biol. Chem. 23*, 14349−14358.
Fárres, J., Wang, T. T. Y., Cunningham, S. J., & Weiner, H. (1995) *Biochemistry 34*, 2592−2598.
Gruff, E. S., & Koch, S. A. (1989) *J. Am. Chem. Soc. 111*, 8762−8763.
Hempel, J., Nicholas, H., & Lindahl, R. (1993) *Protein Sci. 2*, 1892−1900.
Henehan, G. T. M., & Oppenheimer, N. J. (1993) *Biochemistry 32*, 735−738.
Jorgensen, W. L., Chandrasekhar, J., & Madura, J. D. (1983) *J. Chem. Phys. 79*, 926−935.
Jurema, M. W., & Shields, G. C. (1993) *J. Comput. Chem. 14*, 89−104.
Klinman, J. P. (1981) *Crit. Rev. Biochem. 10*, 39−78.
Molecular Simulations, Inc. (1994) Quanta versions 3.3 and 4.0 software, Polygen/MSI Inc., Waltham, MA (currently, Biosym/MSI, San Diego, CA).
Olson, L. P., & Bruice, T. C. (1995) *Biochemistry 34*, 7335−7347.
Palmer, A. G., & Case, D. A. (1992) *J. Am. Chem. Soc. 114*, 9059−9067.
Raber, D. J., & Rodriguez, W. (1985) *J. Am. Chem. Soc. 107*, 4146−4147.
Ramaswamy, S., Eklund, H., & Plapp, B. V. (1994) *Biochemistry 33*, 5230−5237.
Ríos, M. A., & Rodríguez, J. (1992) *J. Comput. Chem. 13*, 860−866.
Ryde, U. (1994) *Int. J. Quantum Chem. 52*, 1229−1243.
Ryde, U. (1995) *Proteins: Struct., Funct., Genet. 21*, 40−56.
Schröder, S., Daggett, V., & Kollman, P. (1991) *J. Am. Chem. Soc. 113*, 8922−8925.
Semichem, Inc. (1994) *Ampac 5.0*, Semichem, 7128 Summit, Shawnee, KS 66216.
Shearer, G. L., Kim, K., Lee, K. M., Wang, C. K., & Plapp, B. V. (1993) *Biochemistry 32*, 11186−11194.
Stewart, J. J. P. (1989a) *J. Comput. Chem. 10*, 209−220.
Stewart, J. J. P. (1989b) *J. Comput. Chem. 10*, 221−264.
Stewart, J. J. P. (1991) *J. Comput. Chem. 12*, 320−341.
Tapia, O., Lamborelle, C., & Johannin, G. (1980) *Chem. Phys. Lett. 72*, 334−341.
Tapia, O., Brändén, C. I., & Armbruster, A. M. (1983) *Quantum Theor. Chem. React. 3*, 97−123.
Tapia, O., Cardenas, R., Andres, J., Krechl, J., Campillo, M., & Colonna-Cesari, F. (1991) *Int. J. Quantum Chem. 39*, 767−786.
van Gunsteren, W. F., & Berendsen, H. J. C. (1977) *Mol. Phys. 34*, 1311−1327.
von Onciul, A., & Clark, T. (1993) *J. Comput. Chem. 4*, 392−400.
Wang, X., & Weiner, H. (1995) *Biochemistry 34*, 237−243.
Wu, Y.-D., & Houk, K. N. (1991) *J. Am. Chem. Soc. 113*, 2353−2358.
Wu, Y.-D., & Houk, K. N. (1993) *J. Org. Chem. 58*, 2043−2045.
Wu, Y.-D., Lai, D. K. W., & Houk, K. N. (1995) *J. Am. Chem. Soc. 117*, 4100−4108.
Zheng, Y.-J., Merz, K. M., & Farber, G. K. (1993) *Protein Eng. 6*, 479−484.

BI952020X